Analysis and Modeling of Film Capacitor Radiation Generic Radiating Model for the Rectangular Capacitors

Walid Labiedh, Bessem Zitouna, Mohamed Tlig, and Jaleleddine Ben Hadj Slama

LATIS, Laboratory of Advanced Technology and Intelligent Systems
ENISo, National Engineering School of Sousse - University of Sousse, Tunisia

Abstract ─ Capacitors are sources of EM field emissions whose characterization is crucial for electronic circuits EMC. This paper presents the modeling of equivalent radiating sources of rectangular film capacitors. It presents and analyses the magnetic near field measured above plastic and polyester capacitors. The measurements are then used by the inverse method to create a radiating source model for the capacitor. The results show a good agreement between the measured cartography and the one obtained when using radiating sources model. Finally, a generic radiating model is proposed for various types of rectangular film capacitors. The generic model is validated using the measurements on a rectangular capacitor. The suggested radiating model accelerates solving the inverse method. It can be used by circuit designers to optimize the placement of capacitors on the printed circuit board to reduce their coupling with other components of the studied system.

Index Terms ─ Electromagnetic compatibility, electromagnetic radiation, film capacitors, inverse problems, near field.

I. INTRODUCTION

In power electronics, the switching frequencies are increasingly high so as to reduce the weight, the volume and the cost of these systems. This rise in frequency is accompanied with an increase in conducted and radiated electromagnetic disturbances. It also has important effects on the behavior of these components at high frequencies. The characterization of the electromagnetic behavior of the various components of power electronics systems is an important step that will serve to better control the electromagnetic compatibility of these systems as early as the design phase [1-4].

There are many researches that have proposed radiating models for components or systems. In fact, concerning systems, [2] put forward a radiating model of a DC-DC converter, referenced as TEN 40-2412. The suggested model was composed of a network of four magnetic dipoles. The study [3] proposed two radiating models of a circuit based on a microcontroller. The first model was based on 53 magnetic dipoles while the second one was based on 517 electric dipoles. For components, [4] put forward a radiating model of the MOSFET. The obtained model was constituted by a magnetic dipole. Two radiating models of a toric self-inductance were suggested in [5]. The first developed model consisted of a large number of dipoles (676 dipoles). It was got by using a modeling approach based on the matrix inversion. The second model was composed of a network of 12 dipoles. Previous, researches have already put forward a radiating model for an inductor [6-7]. The proposed model by [6] consisted of a network of two simple magnetic dipoles. However, the one suggested by [7] was composed of a large number of magnetic and electric dipoles (520 dipoles). The measurements of the electromagnetic radiation were performed as described in [8].

On the other hand, several methods have been developed to model the radiated emissions of components and electrical systems. The study [3] suggested two methods. The first one was based on magnetic dipoles and the second one was based on electric dipoles. The two presented methods required both the amplitude and the phase of the field. The study [4] put forward an electromagnetic inverse method based on the Genetic Algorithms (GA). The method gave good results in the case where the number of searched parameters is not very important; otherwise the method was inefficient when considering calculation time and convergence. For this, the same authors developed in [2] a new approach based on image processing descriptor PZMI, which consisted in processing only a scan window of the measured magnetic field cartography. Another approach was developed by [6-7]. It was based on the matrix calculation.

In this paper, we are interested in radiation of film capacitors. The film capacitors are widely used in the power electronics domain and they are replacing electrolytic capacitors. They particularly permit the improvement of reliability and EMI suppression. Indeed, they are often used in new industrial applications, such as power converters for renewable energy and also for hybrid automotive systems. The film capacitors are mainly characterized by a high insulation resistance, large

Submitted On: October 15, 2020
Accepted On: March 6, 2021
https://doi.org/10.47037/2020.ACES.J.360408

conducted currents and a good stability of its capacitance. These components are generally cumbersome and their radiation certainly affects the overall radiation of the circuits. The electromagnetic field radiated by capacitors creates induced disturbances that may cause a dysfunction to the neighboring circuits. Therefore, the mastery of all the circuit's radiated field is a requirement for the proper functioning of the system. It will be worthwhile to dispose of the radiation model of capacitors.

The literature review of papers related to EMC analysis of discrete capacitors shows few studies dealing only with conducted disturbances across these components and their coupling effects on other neighboring components. Particularly, in [9-12] the authors first studied the electromagnetic coupling between the components of an EMC filter. The filter was composed of two capacitors and two coils. Second, they proposed an automatic method to determine the optimal placement of components and the associated tracks' design. However, these studies treat the coupling in a special single application which is an EMC filter. They were not interested in the capacitors radiation. [12] put forward methods for predicting the distribution of the magnetic field in capacitors. Although, the existence of a magnetic field may seem anecdotal in capacitors who's functioning depends on the electric field, this is not the case because the magnetic field is precisely the cause of imperfections of the capacitors: the equivalent series inductance, the resonant frequencies, the associated losses, and the currents induced in metallization [13].

The aim of the present paper is to propose a radiation model for film capacitors, which has never been proposed before. In the next section, we will present the experimental techniques used to characterize the near field around the capacitors. In the third section, we will analyze the magnetic near field above the capacitors. The modeling method will be explained in the section four. It will be then applied in the following section to develop the radiating models of the studied capacitors. Finally, we will put forward a generic model for all rectangular capacitors.

II. EXPERIMENTAL TECHNIQUES AND CHARACTERIZATION METHOD

A. Excitation circuit

To allow characterization over a wide frequency band, we excite the studied component with a current having a large frequency band similar to the one found in power electronics. Therefore, we propose to insert the component under test in a converter circuit supplied by a voltage equal to 30V and having a duty cycle equal to 0.5 (Fig. 1). The output current of the circuit is of 0.5 A. The switching frequency is 50 kHz.

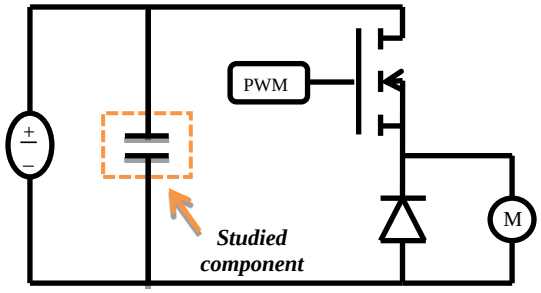

Fig. 1. Chopper circuit where studied component is characterized.

B. Measurements methods

In our study, we utilize only one component of the field radiated by the system under test. Indeed, the use of a single component in a large number of points is quite sufficient for identifying the equivalent source by guaranteeing the uniqueness of the solution [14-15].

Furthermore, the developed radiating model is capable of modeling the electric field as well as the magnetic field. Actually, based on [16-18], we can calculate from the magnetic field, the electric one and vice versa.

Since the method can be applied to any component of the magnetic or electric field, we have used the vertical component Hz. We may also utilize the other tangential components (Hx or Hy). For measuring the magnetic near field, we place a magnetic probe above the device under test. It is a manually made probe, which consists of a 1.6mm radius circular loop connected to the central conductor on one side and to the external shield of a coaxial cable on the other side. To capture the various components of the H field, it is necessary to place the normal of the collinear loop to the desired component.

In our study, we use two methods for measuring the magnetic field around the component. The first method performs the measurements of the near field in the frequency domain and the second one is performed in the time domain.

C. Probe calibration

It is worth noting that the used electronic probes are none other than small sensors or antennas as proposed and implemented in the IRSEEM NF test bench [7-8] [19]. In these studies, the authors suggested a method to validate the accuracy of their magnetic field probes. They measured the radiated magnetic field around a simple circuit which was a conductive wire above a ground plane. The values of the measured field were compared to those calculated theoretically. Thus, the results comparison enabled the validation of the used probes.

Similarly, in this work, to calibrate the magnetic probe, we have used a radiating circuit whose radiation is known theoretically. We compare the measured radiated magnetic field to that calculated by the numerical electromagnetic tool NEC [20] based on the moment's method. The radiating circuit is a rectangular loop of 5 cm length and 3 cm width excited by a sinusoidal voltage of 10V amplitude at a frequency of 5MHz (Fig. 2).

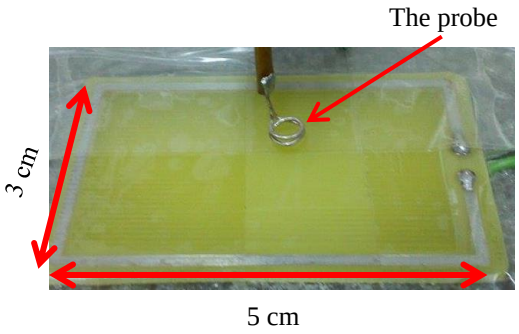

Fig. 2. Loop used for probe calibration.

The simulations and measurements are made at the points located in a horizontal plane at a height of 3 mm above the radiating loop and having dimensions of 5 cm X 3 cm. The calculation step is of 2.5 mm along the X axis and of 1.5 mm along the Y axis (441 measurement points).

Figures 3, 4 and 5 present the magnetic field components Hz, Hx and Hy along the X and Y axis respectively. It shows a good agreement between the measured and calculated curves of Hz component. In order to, have a good signal to noise ratio when measuring Hx and Hy components, we chose measurements lines located at the edge of the emitting loop. Consequently, in some positions of the measuring probe we notice a difference between measurements and simulations due to the edges effects and the coupling effects between the probe and the radiating loop. These phenomena are not significant on the Hz component and therefore do not affect the construction of the model.

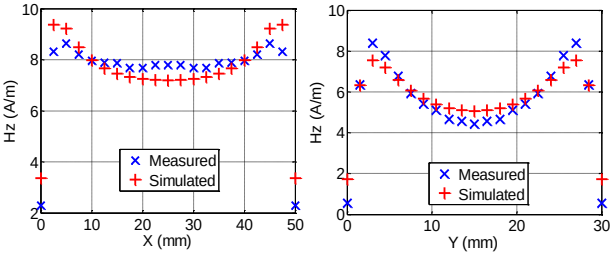

Fig. 3. Hz following X and Y axes respectively for Y = 4.5 mm and X = 25 mm.

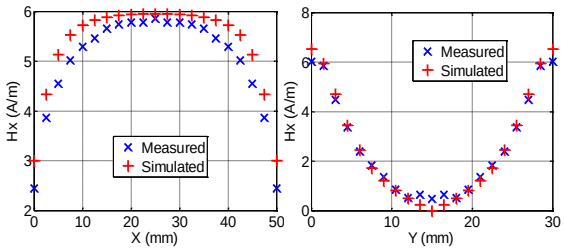

Fig. 4. Hx following X and Y axes respectively for Y = 1.5 mm and X = 25 mm.

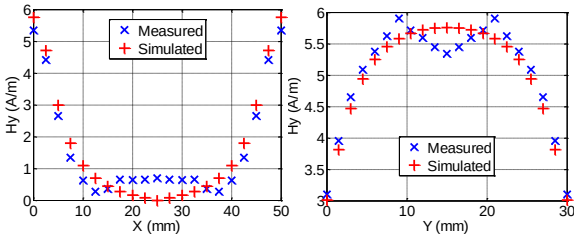

Fig. 5. Hy following X and Y axes respectively for Y = 1.5 mm and X = 25 mm.

In order to examine the electric field rejection capability of our magnetic probe, we have placed it over a transmitting electric antenna where the amplitude of the electric field is important. The observed voltage across the probe is so low that we cannot dissociate it from the noise. Hence, we deduce that our shielded probe rejects very well the electric field and measures the magnetic field with great accuracy.

III. MEASUREMENTS AND ANALYSIS OF POLYPROPYLENE CAPACITOR RADIATION

Measurements are performed in the time domain using a high bandwidth oscilloscope. We have measured the vertical component Hz of the magnetic near-field radiated above a plastic polypropylene capacitor of a 2.2uF capacitance and a maximum voltage of 100V (the capacitor size is15mm x 6mm x 26.5mm). To avoid the interferences caused by the capacitor legs, we have folded the legs of the latter. The probe is located at a distance of 2 mm above the capacitor in a plane whose dimensions are 4cm x 2cm. The displacements are done with a measuring step of 2 mm on the X axis and 1 mm on the Y axis. Thus, we have 400 measurement points. Figure 6 shows the measurement plane and the component under test. It gives a particular point (3,5) position in the measurement plane.

Figure 7 shows the temporal signal measured at the terminals of the magnetic probe once it is situated at the point (3,5): the third position along the X axis and

the fifth position along the Y axis. When analyzing the measured magnetic field signal, we notice the existence of switching transients during the turning on and the turning off of the power component utilized in the chopper.

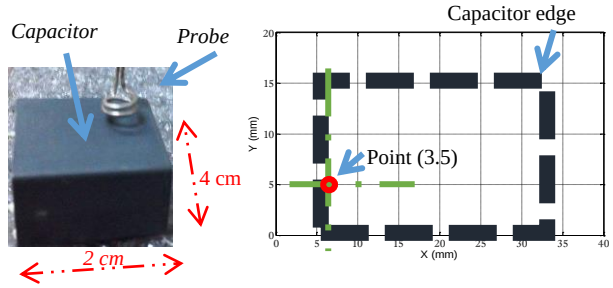

Fig. 6. Measurement plane over component under test.

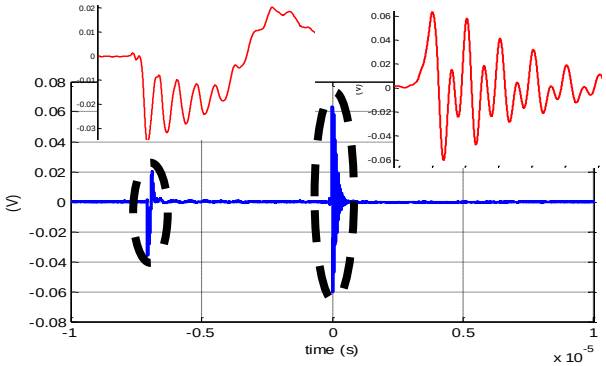

Fig. 7. Measured temporal signal at the terminals of the probe above capacitor under test.

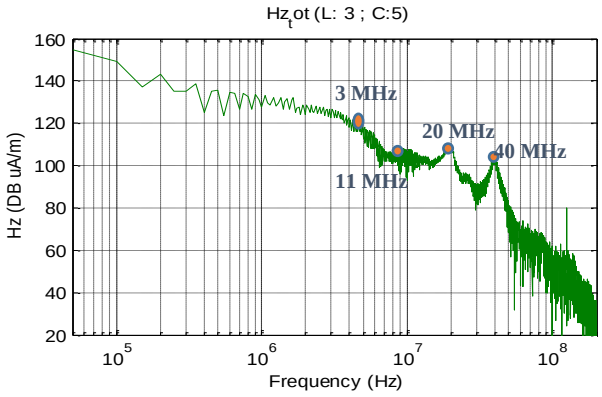

Fig. 8. Spectrum of radiated magnetic field Hz at the terminals of the probe above the studied capacitor at point (3.5).

Figure 8 shows the spectrum analysis of the full temporal signal with both switching phases (closing and opening of the MOSFET in the excitation circuit where our studied component is characterized). That measured above the capacitor at the point of the coordinates (3,5) presented in Fig. 7. By analyzing the spectrum of the measured temporal signal, we notice the appearance of four principal harmonics which have the following frequencies: 3 MHz, 11 MHz, 20 MHz, and 40 MHz. The resonances that appear above the capacitor are principally due to the operating current flowing into the chopper circuit.

We present in Fig. 9 the cartographies of the field above the capacitor at these different frequencies.

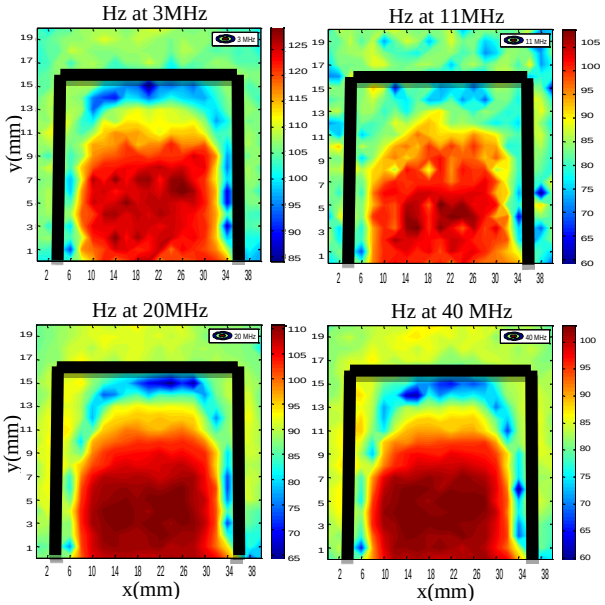

Fig. 9. Cartographies of near field for 3MHz, 11 MHz, 20 MHz, and 40 MHz frequencies.

According to the previous cartographies, it is noted that the distribution of the radiated magnetic field above the capacitor is located on the entire surface of the component as illustrated in Fig. 10.

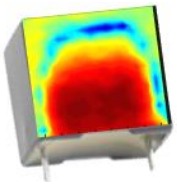

Fig. 10. Distribution of magnetic field above capacitor (frequency equal 20 MHz).

IV. MODELING METHODOLOGY

To develop a radiating model that enables producing a near field equal to that's radiated by the system under test. The modeling methodology given in Fig. 11 is based on a hybrid approach consisting in the coupling between

the electromagnetic inverse method and the Method of Moments (MoM) [21]. The optimization method used in this work is based on genetic algorithm that has been presented in [22-24]. To reduce the convergence time of the electromagnetic inverse method, we take into account the study presented in [22] to choose the optimum parameters of the genetic algorithms. These optimum parameters are given in Table 1.

The equation presented in Table 1 gives the fitness function which ensures the comparison between the estimated and the measured field. It is equal to the sum, on all points of the measured cartography of the relative errors between the measured magnetic near-field and the estimated one.

Table 1: Optimum parameters of genetic algorithms

Fitness Function	Population Size (Np)	Selection Function	Crossover Rate
$Error = \sum_{i=1}^{n} \frac{\lvert H\ measured - H\ estimated \rvert}{H\ measured} \times 100$	Np = 20 × number of parameters of dipoles	Roulette	0.8

These numerical modeling methods depend on the performance of the machines on which they are run and the complexity of the simulated structure. Therefore, very high precision is required; a more powerful PC in order to reduce the computing time is required.

After, the search is launched to find the parameters of the equivalent radiating structure by comparing the measured cartography to the one calculated numerically by the moment's method and using the obtained parameters.

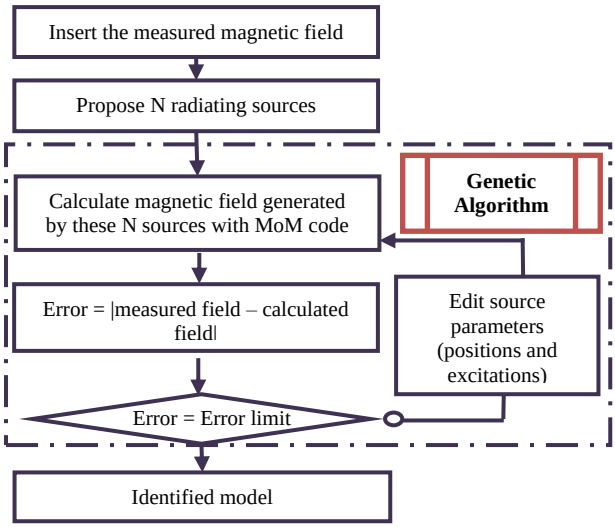

Fig. 11. Flow chart of the modeling approach.

The calculation of the magnetic field generated by the N sources is done through the NEC2D software core which is based on the MoM.

As the capacitor cartographies gather at the radiation of a rectangular loop, the search for models has been launched to find a rectangular current loop using the method based on the coupling between inverse method and the MoM. Each rectangular loop as given in Fig. 12 is characterized by the coordinates of its center (X0, Y0, Z0), its width (w), its length (L), its orientations (φ, θ), the radius (r) of the loop wire, and the current flowing through it.

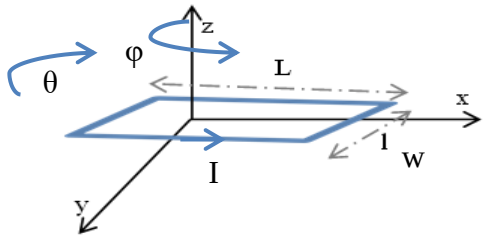

Fig. 12. Rectangular current loop parameters.

V. MODEL FOR THE POLYPROPYLENE CAPACITOR

A. Model research

After presenting the cartographies of the magnetic field radiated by the capacitor in section 3, we apply our approach to find a model that gives the same radiation as that measured over the capacitor. To do this, we used the cartography of the vertical component Hz of the magnetic field at a frequency of 20 MHz. We chose the cartography of 20 MHz because it was the clearest one. The modeling results are shown in Table 2.

Figure 13 shows the position of the identified loop on the capacitor cartography.

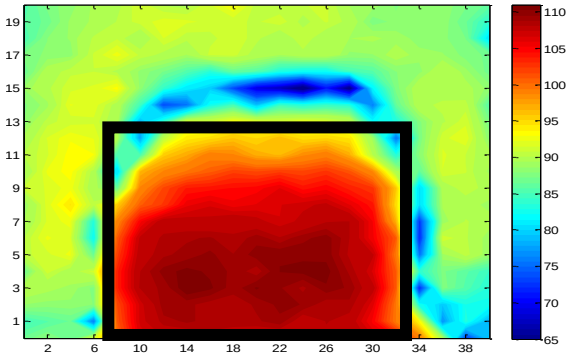

Fig. 13. Obtained loop position.

Table 2: Parameters of the obtained rectangular loop

Center Coordinates (X_0, Y_0, Z_0) (mm)	Loop Dimensions Width, Length (mm)	Orientations Φ, θ (rd)	Conductor Radius R (mm)	Voltage Excitation (V)
3.6; 19; -2.9	12; 23	0; 0	1	0.035

Figure 14 presents the measured and estimated cartographies of the magnetic field vertical component Hz. A reasonable agreement between the two cartographies is observed.

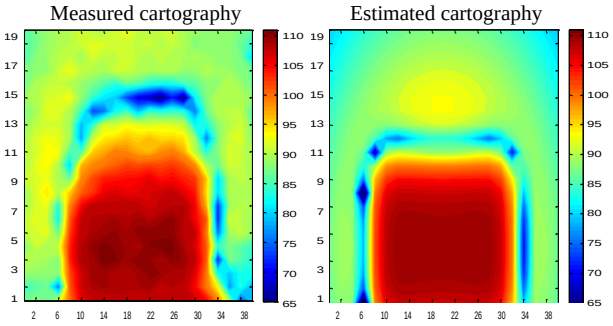

Fig. 14. Measured and estimated cartographies.

B. Model validation

To validate the reconstructed model, we propose to present a comparison between the estimated and measured cartographies for other faces of the capacitor or other components as proposed in [4], [25]. To do this, initially, we perform an experimental measurement of the cartography of the magnetic field on other face of the capacitor (Hx measured). For this, we placed the capacitor vertically and we measured the magnetic field radiated from this face. In the second step, we exploit the estimated parameters to calculate the cartography of the tangential component of the magnetic field (Hx estimated). Figure 15 depicts the layout of the measurements.

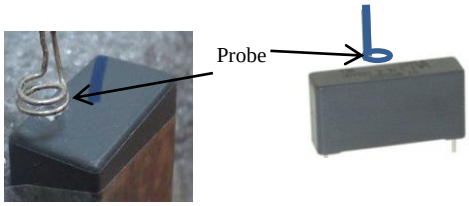

Fig. 15. Measurement of magnetic field over vertically placed capacitor.

The validation of the model is made for the frequency of 20 MHz and at a measurement height of 3 mm. We give in Fig. 16 the measured magnetic field cartography and that's calculated by the model above the vertically placed capacitor.

According to the previous results, the magnetic field reconstructed by the model shows a good accordance with the measured one. These results confirm the existence of an equivalent rectangular current loop in the capacitor. To explain the obtained results, we present in Fig. 17 the internal structure of the capacitor.

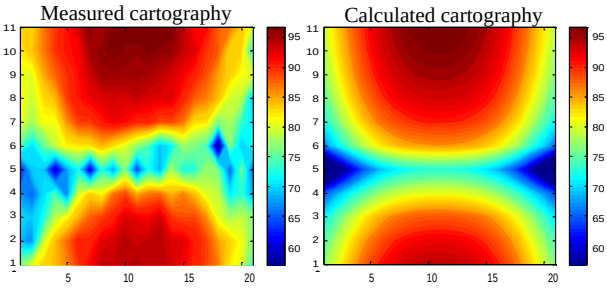

Fig. 16. Cartographies of measured and calculated field above vertically placed capacitor.

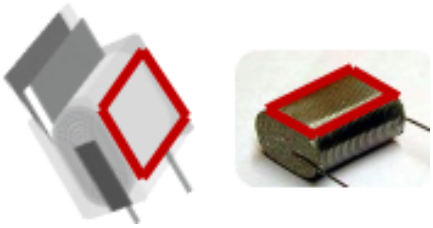

Fig. 17. Film capacitor's internal structure.

The analysis of the internal structure of the film capacitor confirms the obtained equivalent model. Indeed, the surface of the capacitor appears as a rectangular loop.

This current distribution at the capacitor contour is certainly caused by the internal coupling phenomena in the component. This current distribution in the capacitor film is consistent with that introduced in [12-13].

VI. MODEL FOR THE METALLIZED POLYESTER CAPACITOR

A. Measurement of magnetic near-field radiated by polyester capacitors

Based on the frequency measurement method, we measured the vertical component Hz of the magnetic field radiated above a metallized polyester capacitor of a 1μF capacitance and having a maximum voltage of 100V (the capacitor size 14mm x 7mm x 18mm). In order to have exactly only the magnetic field radiated by the capacitor, we bent the legs of the capacitor. The probe was located at a 3 mm distance from the capacitor. The measurements of the magnetic-field were performed in

a plane whose dimensions were 30mm x 20mm with a measuring step of 1.5 mm on the X axis and 1 mm on the Y axis. Figure 18 shows the measurement plane and the component under test.

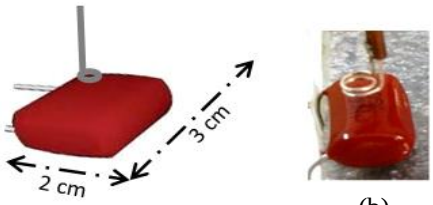

(a) (b)

Fig. 18. (a) Measurement plan and (b) device under test.

After making Fast Fourier transformation (FFT) of the measured signals above the capacitor, we notice that the frequency of 26 MHz has maximum amplitude. We present in Fig. 19 the cartographies of the Hz and Hy components measured at the frequency of 26 MHz.

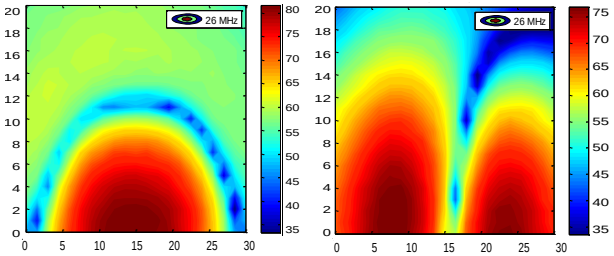

(a) (b)

Fig. 19. Cartographies of the field above the capacitor: (a) Hz and (b) Hy.

B. Radiated-field modelling

As for the polypropylene capacitor, the radiation of the polyester capacitor looks like that of a rectangular loop. We applied the same method exposed previously to the cartography of the measured magnetic field Hz at the frequency of 26 MHz. The modeling result is a rectangular current loop whose parameters are given in Table 3.

Table 3: Parameters of the obtained rectangular loop

Center Coordinates (X_0, Y_0, Z_0) (mm)	**Loop Dimensions Width, Length (mm)**	**Orientations Φ, θ (rd)**	**Conductor Radius R (mm)**	**Voltage Excitation (V)**
1; 15; -3.3	12; 16	0; -0.2	1	0.0017

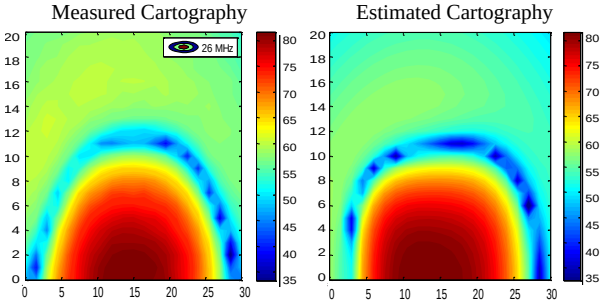

Fig. 20. Measured and estimated the vertical component Hz cartographies of polyester capacitor.

Figure 20 exposes the cartographies of the magnetic field Hz measured and estimated by the obtained model above the capacitor. A good agreement between the two cartographies is observed.

C. Model validation

To validate the obtained model in a better way, we examined the cartographies of the other components of the magnetic field above the capacitor. We specifically compared the measured component Hy of the magnetic field with that calculated using the obtained model.

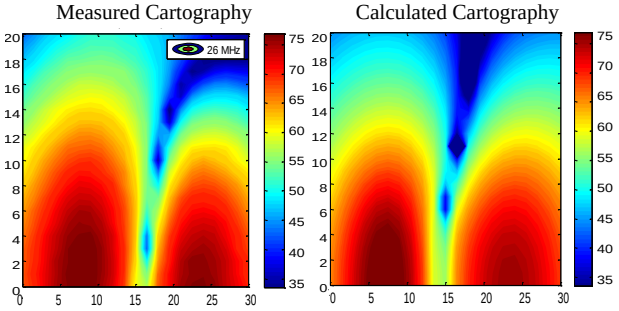

Fig. 21. Cartographies of measured and estimated Hy component of the magnetic field above the capacitor.

Figure 21 show that the magnetic field reconstructed by the model resembles to a great extent the measured magnetic field.

D. Generic model for capacitor

The examination of the results obtained previously allows us to conclude that the equivalent radiating model for the different types of the rectangular film capacitors is a rectangular loop whose parameters depend on the geometry of the capacitor as illustrated in Fig. 22 and explained in equations (1) to (4).

We suggest formulas to determine, using capacitor dimensions, and the size of the source rectangular loop of the generic model.

The center coordinates	= Gravity center of the capacitor
Loop dimensions	$Width_{Generic} \cong 0.8 \times Width_{capacitor}$, (1)
	$Length_{Generic} \cong 0.86 \times Length_{capacitor}$, (2)
Orientations	$\varphi = 0$ (rd) (3)
	θ depends on the position of the capacitor under test relative the x-axis $\cong 0$. (4)
Excitation Voltage	Dependence on the field amplitude

To validate the proposed generic model, we applied it on another rectangular capacitor. Therefore, we measured the magnetic field above a third rectangular capacitor having 2.2μF capacitance and a maximum voltage of 250V (the capacitor size is 25mm x 14mm x 41.5mm).

We performed measurements of the near field cartography above the studied capacitor and then we applied the method based on the coupling of the electromagnetic inverse method with the MoM to find the equivalent model that will be compared to the one obtained by the generic model formulas.

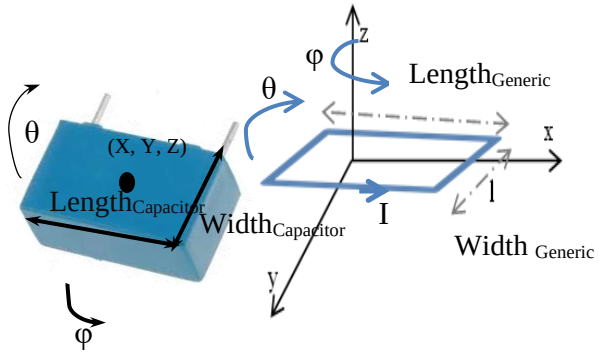

Fig. 22. Capacitor parameters and the analogy with the equivalent loop.

According to Table 4, we notice that the calculated parameters by the formulas of the generic model are very close to those obtained by the inverse electromagnetic method.

Table 4: Parameters of rectangular loop obtained by two methods

Obtained Parameters by Two Methods	Center Coordinates (X_0, Y_0, Z_0) (mm)	Loop Dimensions Width, Length (mm)	Orientations Φ, θ (rd)	Conductor Radius R (mm)	Voltage Excitation (V)	Modeling Time (min.)
Without generic model	2; 26; -7.3	21; 37	0; 0	1	0.0007	62
Generic model	2.3; 25; -7	20; 35.69	0; 0	1	0.00055	8

We observe from the previous table that searching model using the generic model is seven times faster than when being used without the generic model. Indeed, in the generic model we search only one parameter (the excitation voltage) whiles the others parameters are calculated using the formulas given in equations (1) to (4).

Figure 23 shows the components Hy and Hz of the magnetic near-field measured and estimated by the two obtained models above the capacitor under test at a frequency of 27 MHz.

According to the results presented in Fig. 23, the magnetic field reconstructed using the proposed generic model shows an agreement with the measured magnetic field. In fact, in our modeling approach, we are interested in the high amplitudes of the magnetic field (red parts in the cartographies) because they have the most important magnetic field radiated by the component under test. For these values we notice a good agreement between the measured field and the one calculated by the generic model.

Figure 24 presents a comparison between the two models for cuts of the components Hz and Hy along the x-axis. It shows a reasonable agreement between the measured magnetic field and the obtained one with the two models.

The examination of all the obtained results enables us to conclude that the suggested generic model is a slight model that permits, in a very short time, the calculation of the radiation of the different types of the rectangular capacitors.

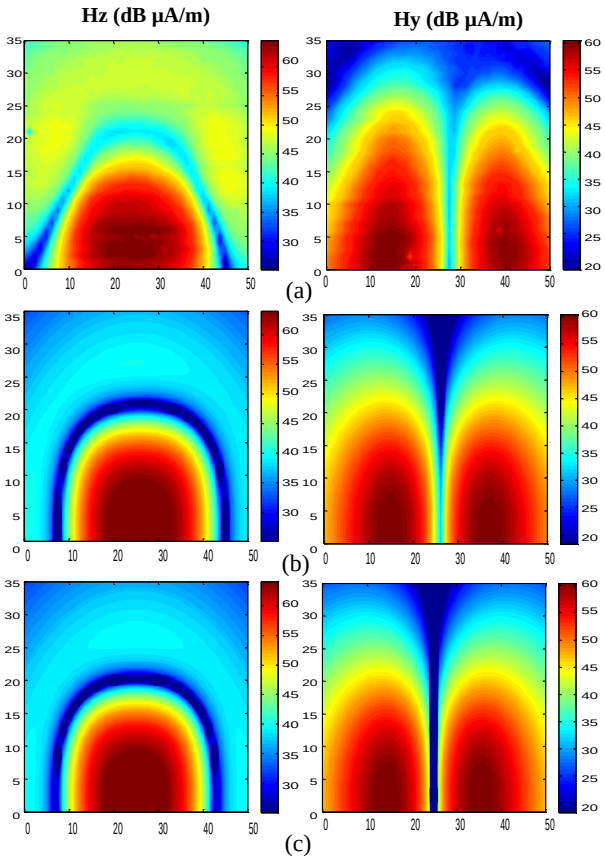

Fig. 23. Cartographies of magnetic field: (a) measured, (b) estimated using inverse method, and (c) using generic model (at frequency of 27 MHz).

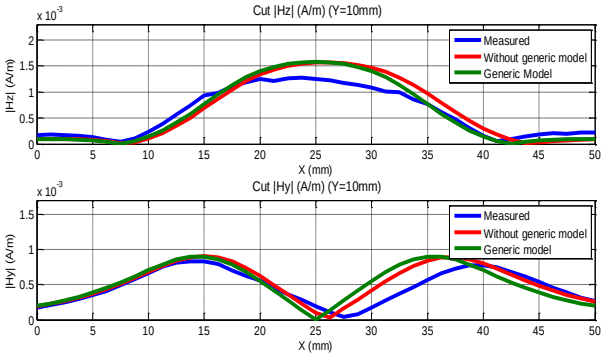

Fig. 24. Comparison of the two models for cuts of Hz and Hy components along the x-axis.

VII. CONCLUSION

Film capacitors are among the larger components on power electronics boards. Therefore, they cause a considerable radiation above all the circuit. In this paper, we have presented the characterization measurements of the magnetic field radiated by different film capacitors utilized in power electronics. We have then used the inverse electromagnetic method based on coupling between the Genetic algorithms and the moment's method to propose models of equivalent radiating sources of these capacitors. A generic radiating model for different types of rectangular film capacitors has been finally put forward and validated using measurements on another capacitor.

This equivalent model is special; hence, its radiation is much more complicated than the one that is usually used by the electromagnetic inverse problem (elementary magnetic and electric dipoles).

The proposed radiating model reduces the number of parameters to be determined by the GA method and consequently reduces the convergence time of the inverse method. It can be utilized by circuit designers to optimize the placement of capacitors on the printed circuit board to reduce their coupling with other components of the studied system.

REFERENCES

[1] J. Ben Hadj Slama and W. Labiedh, "Library of EMC models for passive components and printed circuit board," *Electrotechnical Conference (MELECON), 16th IEEE Mediterranean*, pp. 325-330, Mar. 25-28, 2012.

[2] S. Saidi and J. Ben Hadj Slama, "A near-field technique based on PZMI, GA, and ANN: Application to power electronics systems," *Electromagnetic Compatibility, IEEE Transactions on*, vol. 56, no. 4, pp. 784-791, Aug. 2014.

[3] Y. Vives-Gilabert, C. Arcambal, A. Louis, F. De Daran, P. Eudeline, and B. Mazari, "Modeling magnetic radiations of electronic circuits using near-field scanning method," *Electromagnetic Compatibility, IEEE Transactions on*, vol. 49, no. 2, pp. 391-400, May 2007.

[4] S. Saidi and J. Ben Hadj Slama, "Analysis and modeling of power mosfet radiation," *Progress in Electromagnetics Research M*, vol. 31, pp. 247-262, 2013.

[5] Y. Vives-Gilabert, C. Arcambal, A. Louis, P. Eudeline, and B. Mazari, "Modeling magnetic emissions combining image processing and an optimization algorithm" *IEEE Transactions on Electromagnetic Compatibility*, vol. 51, no. 4, pp. 909-918, Nov. 2009.

[6] P.-E. Levy, C. Gautier, F. Costa, B. Revol, and C. Labarre, "Accurate modeling of radiated electromagnetic field by a coil with a toroidal ferromagnetic core," *Electromagnetic Compatibility, IEEE Transactions on*, vol. 55, no. 5, pp. 825-833, Oct. 2013.

[7] H. Shall, Z. Riah, and M. Kadi, "A 3-D near-field modeling approach for electromagnetic interference prediction," *Electromagnetic Compatibility, IEEE Transactions on*, vol. 56, no. 1, pp. 102-112,

Feb. 2014.

[8] D. Baudry, C. Arcambal, A. Louis, B. Mazari, and P. Eudeline, "Applications of the near-field techniques in EMC investigations," *Electromagnetic Compatibility, IEEE Transactions on*, vol. 49, no. 3, pp. 485-493, Aug. 2007.

[9] T. De-Oliveira, J.-L. Schanen, J.-M. Guichon, and L. Gerbaud, "Optimal stray magnetic couplings for EMC filters," Industry Applications, *IEEE Transactions on*, vol. 49, no. 4, pp. 1619-1627, July-Aug. 2013.

[10] T. De Oliveira, J.-M. Guichon, J.-L. Schanen, and L. Gerbaud, "PEEC-models for EMC filter layout optimization," *Integrated Power Electronics Systems (CIPS), 2010 6th International Conference on*, pp. 1-6, Mar. 16-18, 2010.

[11] H. Chen and Z. Qian, "Modeling and characterization of parasitic inductive coupling effects on differential-mode EMI performance of a boost converter," *Electromagnetic Compatibility, IEEE Transactions on*, vol. 53, no. 4, pp. 1072-1080, Nov. 2011.

[12] E. L. Nativel, T. Talbert, T. Martire, C. Joubert, N. Daude, and P. Falgayrettes, "Near-field electromagnetic tomography applied to current density reconstruction in metallized capacitors," *in IEEE Transactions on Power Electronics*, vol. 20, no. 1, pp. 11-16, Jan. 2005.

[13] C. Joubert, A. Béroual, and G. Rojat, "Magnetic field and current distribution in metallized capacitors," *Journal of Applied Physics*, vol. 76, no. 9, pp. 5288-52931, Nov. 1994.

[14] J. Fan, "Near-field scanning for EM emission characterization," *in IEEE Electromagnetic Compatibility Magazine*, vol. 4, no. 3, pp. 67-73, 3rd Quarter 2015.

[15] X. Gao, J. Fan, Y. Zhang, H. Kajbaf, and D. Pommerenke, "Far-field prediction using only magnetic near-field scanning for EMI test," *in IEEE Transactions on Electromagnetic Compatibility*, vol. 56, no. 6, pp. 1335-1343, Dec. 2014.

[16] Y. Liu, B. Ravelo, and A. K. Jastrzebski, "Calculation of time-domain near field Ex,y,z(t) from Hx,y(t) with PWS and FFT transforms," *in Proc. Int. Symp. Electromagn. Compat*., Roma, Italy, pp. 1-6, Sep. 17-20, 2012.

[17] B. Ravelo, "E-field extraction from H-near-field in time-domain by using PWS method," *Progress Electromagn. Res. B*, vol. 25, pp. 171-189, 2010.

[18] Y. Liu, B. Ravelo, A. K. Jastrzebski, and J. B. Hadj Slama, "Calculation of the time domain z-component of the EM-near-field from the x- and y-components," in *Proc. 41st Eur. Microw. Conf.*, pp. 317-320, Oct. 10-13, 2011.

[19] Y. Vives-Gilabert, C. Arcambal, A. Louis, F. de Daran, P. Eudeline, and B. Mazari, "Modeling magnetic radiations of electronic circuits using near-field scanning method," *IEEE Transactions on Electromagnetic Compatibility*, vol. 49, no. 2, pp. 391-400, 2007.

[20] G. J. Burke and A. J. Poggio, "Numerical electromagnetics code (NEC) - Method of moments," *NOSC TD 116 Part I*, Jan. 1981.

[21] J. Ben Hadj Slama and S. Saidi, "Coupling the electromagnetic inverse problem based on genetic algorithms with moment's method for EMC of circuits," *15th IEEE Mediterranean Electrotechnical Conference MELECON'10*, Malta, pp. 709-714, Apr. 26-28, 2010.

[22] S. Saidi and J. Ben Hadj Slama, "Effect of genetic algorithm parameters on convergence of the electromagnetic inverse method," *8th International Multi-Conference on Systems, Signals & Devices*, pp. 1-5, Mar. 22-25, 2011.

[23] Z. Javad, Y. Cai, and N. Ojaroudi, "UWB slot antenna with band-notched property with time domain modeling based on genetic algorithm optimization," *Applied Computational Electromagnetics Society Journal*, vol. 31, no.8, pp. 926-932, Aug. 2016.

[24] Zitouna, B., Ben Hadj Slama, J. , "Enhancement of time-domain electromagnetic inverse method for modeling circuits radiations," *IEEE Trans. Electromagn. Compat., 58, (2), pp. 534–542, 2016.*

[25] B. Zitouna and J. Ben Hadj Slama, "Time domain inverse method based on the near field technique to solve electromagnetic interference problems: Application to an AC/DC flyback converter," *IET Power Electronics*, vol. 11, no. 13, pp. 2133-2139, June 2018.